ISBN: 978-3-95450-253-0 ISSN: 2673-5571 doi:10.18429/JACoW-HB2023-TUA2C2

RECENT ADVANCES IN THE CERN PS IMPEDANCE MODEL AND INSTABILITY SIMULATIONS

S. Joly*,[1], M. Migliorati[1,2], University of Rome 'La Sapienza', Roma, Italy
G. Iadarola, N. Mounet, B. Salvant, C. Zannini, CERN, Geneva, Switzerland
[1]also at CERN, Geneva, Switzerland
[2]also at Istituto Nazionale di Fisica Nucleare, Roma, Italy

Abstract

Transverse instability growth rates in the CERN Proton Synchrotron (PS) are studied thanks to the recently updated impedance model of the machine. Using this model, macroparticle tracking simulations were performed with a new method well-suited for the slicing of short wakes, which achieves comparable performance to the originally implemented method while reducing the required number of slices by a factor of 5 to 10. Dedicated beam-based measurement campaigns were carried out to benchmark the impedance model. Until now, the model underestimated instability growth rates at injection energy. Thanks to a recent addition to the impedance model, namely the kicker magnets' connecting cables and their external circuits, the simulated instability growth rates are now comparable to the measured ones.

INTRODUCTION

A horizontal instability appeared in the PS at injection energy on operational LHC-type beams (of longitudinal emittance $_1$ = 2 eV.s) during the gradual beam parameters ramp-up to reach LIU (LHC Injectors Upgrade project) specifications [1]. Once the instability was mitigated by correcting chromaticity, exhaustive instability growth rates measurements were performed with the aim to continue the benchmark of the post-LIU PS impedance model with beam-based measurements [2]. It turned out that the current model was not able to reproduce the instability through PyHEADTAIL [3] simulations: its growth rates were underestimated. Nonetheless, it provided valuable insight on the origin of the discrepancy and pointed to a missing impedance source. In this contribution, the transverse impedance frequency range responsible for the instability is narrowed down thanks to the measured instability intra-bunch motion. Then, a candidate impedance contribution missing in the model for this frequency range is studied: the connecting cables and external circuits of the kicker magnets. An analytical model based on the transmission line theory is derived to model this impedance contribution. Before performing macroparticles tracking simulations to assess the impact of this new contribution, a novel method to compute the wake kick in macroparticles tracking codes is proposed to speed up simulations. Finally, simulations using the updated model are compared with beam-based measurements.

* sebastien.joly@cern.ch

MEASUREMENTS OF THE FLAT BOTTOM HORIZONTAL INSTABILITY

The instability characterization and the mitigation strategies to tackle it were presented in [4]. Following the instability mitigation efforts, numerous instability growth rate measurements were performed while deactivating the transverse feedback and using a single bunch. The horizontal chromaticity was set to positive ($Q'_x = 0.6$ when the instability was observed for the first time), zero and negative values during the measurements. Simulations failed at reproducing the beam-based measurements as they underestimated the instability growth rates by a factor 5 to 10. Subsequently, an investigation started aiming at understanding the origin of this discrepancy.

Horizontal Instability Characterisation

During the measurements campaign, instability growth rates were measured as well as the instability intra-bunch motion. In the PS, the bunch centroid and intra-bunch motion can be observed by means of a wide-band pick-up. This device allows acquiring the longitudinal and transverse motion within a specified time interval spanning between a single bunch length to a revolution period. Observing in parallel the longitudinal and transverse signals allows us to identify the number of nodes in the transverse pattern, as well as a potential asymmetry between the head and the tail. The longitudinal and transverse motions of a bunch at the beginning of the exponential increase of the beam centroid were measured with the wide-band pick-up over 50 acquisitions every 3 turns. Additionally, the instability power spectrum is computed by means of a Fourier Transform using the NEFFINT [5,6] algorithm. Both the intra-bunch motion and power spectrum are displayed in Fig. 1. Each acquisition spectrum is computed and their average plotted in white dashed lines in the plots. The instability intra-bunch motion is characterized by a mode-0-like envelope (no node) featuring an asymmetry between head and tail of the bunch. Its resulting power spectrum exhibits three main peaks around 0, 1 and 3 MHz.

The peaks observed in the power spectrum might correspond to resonant modes in the impedance spectrum. As the power spectrum is the frequency domain equivalent of the transverse oscillations, it allows to quantify the frequencies of interest when overlapped with the impedance spectrum. In the following we will investigate this possibility.

ISBN: 978-3-95450-253-0 ISSN: 2673-5571 doi:10.18429/JACoW-HB2023-TUA2C2

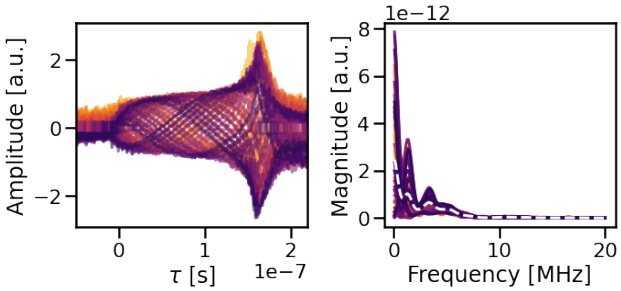

Figure 1: Measured instability transverse oscillations (left) and transverse power spectrum (right) over 50 acquisitions. Horizontal chromaticity ($Q'_x = 0.6$) is set to the value measured at the occasion of the first observation of the instability in the machine. The average transverse power spectrum over all the acquisitions is represented by a dashed white line.

Identification the Missing Impedance Source

Based on Vlasov equation [7], the effects of transverse impedance on beam dynamics such as tune shift or instability growth rates result from the sum of the betatronic lines along the overlap of the impedance and unstable mode spectra. Thus, by overlapping the unstable mode power spectrum from Fig. 1 on top of the PS impedance spectrum, candidates for the impedance contributions responsible for the instability can be identified as shown in Fig. 2.

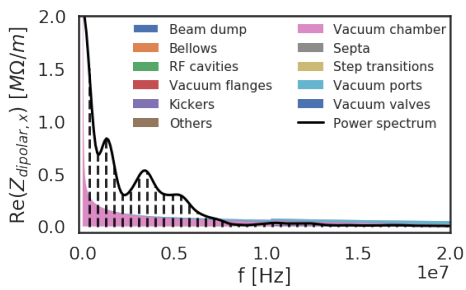

Figure 2: Overlap of the power spectrum measured for Q_x = 6.225 and Q'_x = 0.6 (black line, from Fig. 1) with the impedance spectrum. The betatronic lines, spaced by f_0, are represented by dashed lines.

The dominant contribution in the impedance spectrum in the power spectrum frequency range is the vacuum chamber impedance. The vacuum ports contribution remains negligible for frequencies lower than 10 MHz. We noticed that the frequency range matches the one of the PS kicker magnet BFA09S connecting cables impedance [8]. Therefore, the kickers magnets connection cables and their external circuits are a candidate to explain the impedance missing in the PS impedance model.

IMPEDANCE OF THE PS KICKER MAGNETS CONNECTION CABLES AND THEIR EXTERNAL CIRCUITS

The electromagnetic fields induced by a bunch of charged particles travelling through a kicker magnet can couple with the kicker core and external circuit through the busbar. The external circuits of a kicker magnet includes the cables, ferrite, filters and termination load. The coupling with the external circuit leads to an additional contribution to the beam coupling impedance of the kicker magnet. This contribution leads to longitudinal and dipolar impedance components, due to the location of the cables port as well as the geometry of the cables. It is limited to the MHz range due to attenuation properties of the connecting cables. The external circuits impedance can be calculated analytically by approximating the magnet as an ideal transformer and using the resulting circuit model of the magnet and external circuits as pictured in Fig. 3. This procedure has been applied in the past to the CERN Proton Synchrotron Booster [9], the Oak Ridge National Laboratory Spallation Neutron Source (SNS) kickers [10] and the Super Proton Synchrotron (SPS) kickers [11]. Here, the formalism developed by C. Zannini [11] is expanded to account for a transmission line with losses, the impact of ferrite around portions of cables and the presence of RC filters in the external circuits.

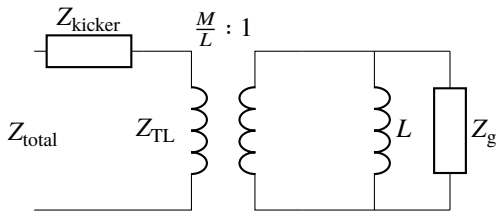

Figure 3: Schematic of the circuit model of a kicker magnet as an ideal transformer [11].

Transmission Line Theory

The impedance contribution from the connecting cables and external circuits Z_{TL} is calculated from the kicker inductance L, self inductance M and the external circuits impedance Z_{g}. The external circuits impedance is expressed using the transmission line theory, which provides a framework to study the behaviour of signals propagating through conductive mediums.

Z_{g} can account for ferrite (approximated as an inductor), filters or propagation through the connecting cables by adding the respective impedances accordingly to the equivalent circuit of the kicker magnet considered. For example, the propagation along the connecting cables terminated by a load can be expressed using the Telegrapher's equations:

$$Z_{\mathrm{g}}(z) = Z_0 \frac{Z_{\mathrm{L}} + Z_0 \tanh(kz)}{Z_0 + Z_{\mathrm{L}} \tanh(kz)}, \qquad (1)$$

where Z_{L} is the load or termination impedance of the line, Z_0 the characteristic impedance of the line, k the propagation

ISBN: 978-3-95450-253-0 ISSN: 2673-5571 doi:10.18429/JACoW-HB2023-TUA2C2

constant and z the position along the line. By replacing z by the length of the line l, the total impedance of the connecting cables can be obtained. The formulation used is general and allows to take into account losses along the line.

The generalized impedance originating from the coupling between the connecting cables and external circuits with the kicker is defined as:

$$Z_{\mathrm{TL}}(x, x_0) = \frac{M(x)M(x_0)}{L^2} \frac{j\omega L Z_{\mathrm{g}}}{j\omega L + Z_{\mathrm{g}}}, \tag{2}$$

where x is the transverse position at which the impedance is evaluated and x_0 the position of the bunch in the kicker magnet. An estimation of the cable inductance and self inductance can be found in [9] for H and C-shape magnets and plugged in Eq. 2 to derive the longitudinal impedance:

$$Z_{\mathrm{l}} = Z_{\mathrm{TL}}|_{x=x_0=0} = \begin{cases} 0 & \text{(H-shape magnet)} \\ \frac{1}{4}\frac{j\omega L Z_{\mathrm{g}}}{j\omega L + Z_{\mathrm{g}}} & \text{(C-shape magnet),} \end{cases} \tag{3}$$

where only H-shape magnets ensure a zero longitudinal impedance.

Then, the horizontal impedance is calculated by applying the Panofsky-Wenzel theorem:

$$Z_{\mathrm{x}} = \frac{c}{\omega} \frac{\partial^2 Z_{\mathrm{TL}}}{\partial x \partial x_0}|_{x=x_0} = \frac{c}{4\omega a^2} \frac{j\omega L Z_{\mathrm{g}}}{j\omega L + Z_{\mathrm{g}}}. \tag{4}$$

The resulting horizontal impedance is independent from the magnet's geometry and yields the same formula for H-shape and C-shape magnets.

Overall Impact on Impedance

The new impedance contribution is characterized by a broadband behaviour surpassing vacuum chamber impedance above 1 MHz, as shown in Fig. 4. In addition, its maximum amplitude frequency coincides with the 3 MHz peak of the power spectrum. The sharp peaks present in the impedance are caused by the open termination of a kicker cable (BFA09S).

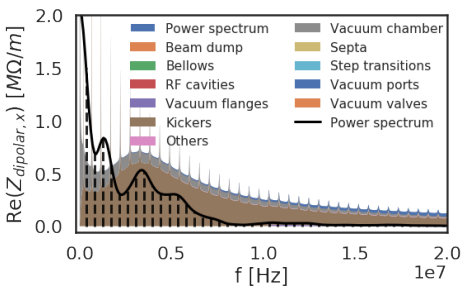

Figure 4: Overlap of the measured power spectrum (black line, from Fig. 1) with the updated impedance spectrum for $Q_x = 6.225$ and $Q'_x = 0.6$. The betatronic lines, spaced by f_0, are represented by dashed lines.

SIMULATIONS OF THE PS FLAT BOTTOM HORIZONTAL INSTABILITY

At injection, a PS bunch length typically varies between 140 and 200 ns whereas the vacuum chamber wake function varies considerably over less than 0.5 ns. One of the shortcomings of the current wake kick implementation, when dealing with such different time scales, is unmanageable simulation times. In the following we address this limitation, before assessing the impact of the kickers cables additional impedance contribution.

Wake Kick Calculation in Tracking Codes

The effect of wakefields on beam dynamics is expressed by the Lorentz force of the resonating electromagnetic fields produced by a bunch of charged particles after their passage in an accelerator element. The integral of the Lorentz force over the element length yields the longitudinal and transverse momentum kicks. For example, the momentum kick caused by a dipolar force is calculated from the convolution of the dipolar wake function with the bunch longitudinal distribution as follows (here in horizontal):

$$\Delta p(z) = -\frac{q}{m_{\mathrm{p}}\gamma\beta^2 c^2} \int_{z'=-\infty}^{\infty} \lambda(z')\langle x(z-z')\rangle w(z-z')dz', \tag{5}$$

where $\langle x(z)\rangle$ is the average horizontal position of the particles along the bunch, z the longitudinal position of the particle experiencing the force, q the elementary charge, m_{p} the mass of the proton, β the relativistic beta, γ the Lorentz factor, c the speed of light in vacuum, $w(z)$ the dipolar (horizontal) wake function and $\lambda(z)$ the beam longitudinal distribution.

Macroparticles tracking codes rely on a discrete representation of a bunch instead of a continuous distribution. On top of that, the bunch is typically sliced longitudinally to compute the wake convolution, as we will see below.

Stepwise Wake Kick Computation

A macroparticle is defined by an ensemble of particles sharing their macroscopic representation in terms of overall charge, energy and position. Once a beam is expressed as a body of macroparticles, it is longitudinally sliced along an equidistant grid and each macroparticle placed in the slice corresponding to its longitudinal position. As a result, for dipolar wakes an unique kick can be applied to each slice. Rewriting Eq. 5 with macroparticles and slices, yields:

$$\Delta p_{\mathrm{i}} = -\frac{q^2}{m_{\mathrm{p}}\gamma\beta^2 c^2} \sum_{n=i+1}^{N_{\mathrm{slices}}} N_{\mathrm{n}} \bar{x}_{\mathrm{n}} w_{\mathrm{n-i}}, \tag{6}$$

where N_{slices} is the number of slices considered, N_{n} expresses the number of macroparticles in the slice n, $\bar{x}_{\mathrm{n}}$ the horizontal centre of mass position of the slice n and $w_{\mathrm{n-i}}$ the wake function for z corresponding to the distance between the center of the slices n and i (the latter being the one for which the kick is evaluated). Note that here, the wake from behind i is neglected.

ISBN: 978-3-95450-253-0 ISSN: 2673-5571 doi:10.18429/JACoW-HB2023-TUA2C2

Two requirements arise from this approach. First, the slicing must be chosen sufficiently fine to evaluate the wake function behaviour correctly, the key point being that the granularity of the approach does not go below the slice level. Then, an adequate number of macroparticles per slice needs to be simulated to prevent statistical noise effects from undersampling, as warned in [12]. Consequently, a single simulation of the PS fulfilling both requirements (i.e., 8000 slices and 5.6 M macroparticles lasts more than two weeks.

Novel Integrated Wakefield Technique

To address the above limitation, efforts have been made to rethink the way the wake kick is evaluated, in particular the integration over the slices. The main challenge lies in finding a strategy to account for the full information of the wake function inside a slice instead of evaluating it at the centre position of the slice. An elegant method, initially proposed by G. Iadarola, is to make use of the integrated wake function over each slice. Previous equation Eq. 5 can be rewritten as a sum of integrals over each slice. Assuming $N_{\mathrm{n}}\bar{x}_{\mathrm{n}}$ can be considered constant in each slice, it can be taken out of the integral leading to:

$$\Delta p_{\mathrm{i}} = -\frac{q^2}{m_{\mathrm{p}}\gamma\beta^2c^2}\times \sum_{n=i+1}^{N_{\mathrm{slices}}} N_{\mathrm{n}}\bar{x}_{\mathrm{n}}\int_{z'=(n-\frac{1}{2})\Delta z}^{(n+\frac{1}{2})\Delta z}\frac{w(z_{\mathrm{i}}-z')}{\Delta z}dz', \tag{7}$$

where Δz is the slice width. This assumption holds provided that the longitudinal and transverse oscillation patterns of the bunch are longer than the slice width, i.e. that the number of slices is significantly larger than the number of oscillations.

Comparison Between the Two Methods

In order to benchmark both methods, they are applied to the PS at injection energy, including only the vacuum chamber wake, which is both the dominant contribution and the one requiring most slices to be fully resolved.

The wake kick calculated for an increasing number of slices with the stepwise and integrated methods is shown in Fig. 5. The stepwise method reaches convergence for approximately 5000 slices, while the integrated method yields almost the same wake kick for 50 slices and fully converges for 500 slices. In this example, a tenfold reduction in the required number of slices is reached thanks to the integrated method.

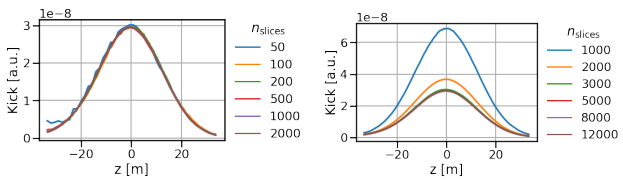

Figure 5: Wake kick comparison between the stepwise (left) and the integrated methods (right).

The integrated method has been routinely employed for PS simulations, effectively reducing the simulation time from a week to 8 h.

Comparison Between Beam-based Measurements and Simulations with the Updated Impedance Model

Simulations are performed with PyHEADTAIL for the three chromaticities for which instability growth rates were measured in the PS. A comparison between measurements and simulations with and without the kickers cables impedance contribution can be seen in Fig. 6. Simulations reproduce the measured growth rates only when the new impedance contribution is included and otherwise underestimate them. This confirms the assumption the instability was driven by an impedance missing from the impedance model in the MHz frequency range. Furthermore, the kickers cables are a good candidate for the missing impedance source.

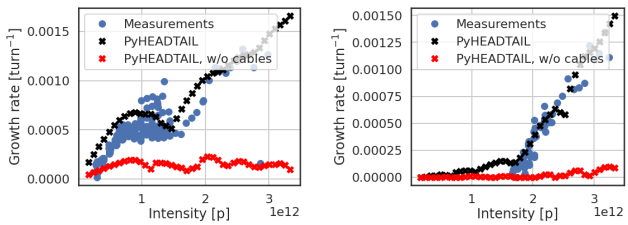

Figure 6: Comparison between measured and simulated instability growth rates for $Q'_x = 0.6$ (left plot) and $Q'_x = -1.2$ (right plot).

CONCLUSION

The measured instability power spectrum proved to be a useful tool in narrowing down the frequency range responsible for an unexpected instability observed at low energy in the PS. An analytical model of the PS kicker magnets connecting cables and external circuits was developed and found to generate a significant source of impedance. Macroparticles tracking simulations were performed using a novel wake kick calculation method, which allowed to significantly reduce the simulation time. The impedance contribution from the kickers has a significant impact on beam dynamics and its addition to the PS impedance model allows simulations to reproduce the growth rate measurements with quite good accuracy.

ACKNOWLEDGEMENTS

The author would like to warmly thank the PS operation team for his help during the growth rates measurements.

REFERENCES

[1] A. Huschauer *et al.*, "Beam Commissioning and Optimisation in the CERN Proton Synchrotron After the Upgrade of the LHC Injectors", in *Proc. IPAC'22*, Bangkok, Thailand, Jun.

ISBN: 978-3-95450-253-0 ISSN: 2673-5571 doi:10.18429/JACoW-HB2023-TUA2C2

2022, pp. 54–57.
doi:10.18429/JACoW-IPAC2022-MOPOST006

[2] S. Joly, B. Salvant, G. Imesch, M. Delrieux, N. Mounet, and M. Migliorati, "Impedance-induced beam observables in the CERN Proton Synchrotron", in *Proc. IPAC'23*, Venice, Italy, May 2023, pp. 3454–3457.
doi:10.18429/JACoW-IPAC2023-WEPL149

[3] PyHEADTAIL macroparticle tracking code,
https://github.com/PyCOMPLETE/PyHEADTAIL

[4] S. Joly, B. Salvant, G. Imesch, M. Delrieux, N. Mounet, and M. Migliorati, "Overview of transverse instabilities in the CERN Proton Synchrotron", in *Proc. IPAC'23*, Venice, Italy, May 2023, pp. 3450–3453.
doi:10.18429/JACoW-IPAC2023-WEPL148

[5] Non-equidistant Filon Fourier integration (NEFFINT) algorithm,
https://neffint.readthedocs.io/en/latest/

[6] N., Mounet, "The LHC transverse coupled-bunch instability", Ph.D. thesis, EPFL, Lausanne, Switzerland, 2012.

[7] A. W. Chao, *Physics of collective beam instabilities in high-energy accelerators*, Wiley series in beam physics and accelerator technology, May 1993.

[8] C. Zannini, presented at the 40th Impedance Working Group Meeting, https://indico.cern.ch/event/915543/

[9] G. Nassibian and F. Sacherer, "Methods for measuring transverse coupling impedances in circular accelerators", *Nucl. Instrum. Methods*, vol. 159, no. 1, pp. 21–27, 1979.
doi:10.1016/0029-554X(79)90323-9

[10] D. Davino and H. Hahn. "Improved analytical model of the transverse coupling impedance of ferrite kicker magnets.", *Phys. Rev. Spec. Top. Accel. Beams*, vol. 6, no. 1, p. 012001, 2003. doi:10.1103/PhysRevSTAB.6.012001

[11] C. Zannini, "Electromagnetic simulation of CERN accelerator components and experimental applications", Ph.D. thesis, EPFL, Lausanne, Switzerland, 2013.

[12] A. Oeftiger, "An Overview of PyHEADTAIL", CERN, Geneva, Switzerland, Rep. CERN-ACC-NOTE-2019-0013, Apr. 2019.